Neoplasia 50 (2024) 100980

Contents lists available at ScienceDirect

Neoplasia

journal homepage: www.elsevier.com/locate/neo

Original Research

Single cell analysis unveils the commonality and heterogeneity between nasopharyngeal and oropharyngeal carcinoma

Liping Wang [a,1], Shuang Li [b,1], Xinran Li [a,1], Guangzheng Zhuo [a], Qian Zhang [a], Guohong Liu [c,*], Yunbao Pan [a,**]

[a] Department of Laboratory Medicine, Zhongnan Hospital of Wuhan University, Wuhan University, Wuhan 430071, PR China
[b] Department of Otolaryngology Head and Neck Surgery, Zhongnan Hospital of Wuhan University, Wuhan 430071, PR China
[c] Department of Radiology, Zhongnan Hospital of Wuhan University, Wuhan University, Wuhan 430071, PR China

ARTICLE INFO

Keywords:
Nasopharyngeal carcinoma
Oropharyngeal carcinoma
Tumor microenvironment
Cellular heterogeneity
Intercellular communication

ABSTRACT

Nasopharyngeal carcinoma (NPC) and oropharyngeal carcinoma (OPC) are subtypes of head and neck cancer with different treatment effects due to the heterogeneity of tumor microenvironments. This study was to investigate the distinctive tumor microenvironments of NPC and OPC. Analyzing single-cell data from 10 cases of each subtype, we reveal significant differences in cellular composition, with NPC microenvironment dominated by T/NK and B cells, and OPC characterized by prevalent epithelial cells and fibroblasts. Dynamic transitions of CD8 T cells are observed in both tumor types, involving shifts from naivety to cytotoxicity, proliferation, and eventual exhaustion/exhausted states. Additionally, Tregs exhibit heightened proliferative abilities in later developmental stages, concomitant with exhaustion. These highly proliferative T cells and Tregs manifest elevated glycolysis and lactate metabolism activities. Furthermore, we explore intercellular communication between glycolytic malignant epithelial cells and these proliferative T cells. These findings offer comprehensive insights into the heterogeneity of tumor microenvironments and provide a solid foundation for future therapeutic strategies and targeted interventions.

1. Introduction

Head and neck cancers (HNCs) encompass a heterogeneous group of malignancies that arise in the upper aerodigestive tract, with nasopharyngeal carcinoma (NPC) and oropharyngeal carcinoma (OPC) being prominent subtypes. Despite advancements in diagnosis and treatment, HNCs remain a significant global health burden due to their complex etiology, aggressive nature, and limited therapeutic options [1]. The tumor microenvironment (TME) plays a pivotal role in shaping cancer progression and therapeutic responses, particularly through its interactions with immune cells [2]. Recent advances in single-cell sequencing technologies have provided unprecedented insights into the cellular and molecular intricacies of the TME, offering an opportunity to unravel the underlying mechanisms governing tumor-immune interactions in HNCs.

In the realm of HNCs, NPC and OPC present captivating subjects for investigation due to their unique anatomical locations, distinct risk factors, and varying clinical behaviors. While NPC is endemic in specific regions and closely linked to Epstein-Barr virus infection [3], OPC has garnered attention for its association with human papillomavirus [4]. Despite these differences, both subtypes share commonalities in treatment challenges and potential immune evasion mechanisms. Conventionally, surgery and chemoradiotherapy are used for early-stage NPC and OPC patients, yielding favorable efficacy and prognosis. However, delayed diagnosis often leads to advanced stages [3,5]. For advanced cases, chemoradiotherapy extends survival but with notable side effects. Precision medicine has introduced immune checkpoint inhibitors (anti-PD-1/PD-L1) in clinics, showing promise when combined with traditional treatments [6,7]. Yet, varying individual responses limit efficacy [8].

* Corresponding author at: Department of Radiology, Zhongnan Hospital of Wuhan University, Wuhan University, No.169 Donghu Road, Wuchang District, Wuhan, 430071, PR China.
** Corresponding author at: Department of Laboratory Medicine, Zhongnan Hospital of Wuhan University, Wuhan University, No.169 Donghu Road, Wuchang District, Wuhan, 430071, PR China.
E-mail addresses: liuguoh@outlook.com (G. Liu), panyunbao@outlook.com (Y. Pan).
[1] Equally contribution and co-first authors.

https://doi.org/10.1016/j.neo.2024.100980
Received 14 November 2023; Accepted 14 February 2024

NPC and OPC originate from anatomically adjacent sites, yet they are driven by distinct viral oncogens and different cancer stem cells [9]. This underscores the need to explore both their similarities and differences in detail. As immunotherapy emerges as a promising modality for cancer treatment, elucidating the differential immune cell composition and function between NPC and OPC may provide valuable clues for optimizing therapeutic strategies. In this study, we performed a comprehensive analysis of single-cell sequencing data to characterize the immune landscapes of NPC and OPC tumors. By delineating the distinct immune cell populations and their functional attributes within these tumors, we aim to uncover the intricate interplay between tumor cells and the immune cells in the context of HNCs. Through this investigation, we seek to enhance our understanding of the immune dynamics within the TME of NPC and OPC, facilitating the development of more specific and effective immunotherapeutic interventions. Our findings may inform the design of novel treatment approaches tailored to the unique immunological profiles of these HNC subtypes. Ultimately, the insights gained from this study may pave the way for improved clinical outcomes and a brighter future for patients afflicted with NPC and OPC.

2. Materials and methods

2.1. Data acquisition and quality control

We obtained the single-cell sequencing data of 10 NPC (GSE162025) and 10 oropharyngeal squamous cell carcinoma (OPSCC) (GSE182227, cell number per sample $>$ 1000) tumor tissue samples from the GEO database (https://www.ncbi.nlm.nih.gov/geo/). The expression matrices of NPC and OPC were merged and converted into Seurat objects using the Seurat package (v4.3.0). Low-quality cells and potential doublets were filtered out, with the criteria: nFeature_RNA $>$ 300 & nFeature_RNA $<$ 6000 & percent.mt $<$ 10 & percent.HB $<$ 1. After filtering, 122891 cells were used for subsequent data normalization and scaling. The gene expression matrix was log-transformed using NormalizeData. VariableFeatures (n=3000) were identified using FindVariableFeatures. The data was scaled using ScaleData. PCA was performed on the scaled gene expression matrix of highly variable genes for dimensionality reduction. Harmony (v0.1.1) was used for batch correction.

2.2. Cell clustering

The FindNeighbors and FindClusters functions were used for cell clustering. The clustered cells were reduced to a 2D UMAP plot for visualization using RunUMAP. Based on known marker genes, the clusters were identified as B cells, endothelial cells, epithelial cells, fibroblasts, mast cells, myeloid cells, and T/NK cells. Next, clusters of interest (T/NK cells and epithelial cells) were selected for a second round of clustering (data normalization, highly variable gene identification, data scaling, batch correction, and re-clustering) to obtain refined subgroups.

2.3. Functional enrichment and scoring

Gmt files (h.all.v2022.1.Hs.symbols.gmt and c2.cp.kegg.v2022.1.Hs.symbols.gmt) were obtained from the Molecular Signatures Database (https://www.gsea-msigdb.org/gsea/msigdb/index.jsp). GSVA (v1.46.0) was used to perform functional enrichment analysis on the cell clusters. Differential analysis of pathway activity scores between NPC and OPC was performed using limma (v3.54.0). Pathways with adjusted $P < 0.05$ and absolute logfc $>$ 0.15 were selected and visualized as a heatmap using ComplexHeatmap (v2.14.0). AddModuleScore function was used to calculate module scores for each cell. Score differences between NPC and OPC were compared using Wilcoxon test ($P < 0.05$ as significant). Module scores included Exhaustion, Cytotoxicity, Proliferation, Naivety, IL2R, and Co-stimulatory. AUCell was used to obtain the glycolysis (MODULE_306) and lactate metabolism (GOBP_LACTATE_METABOLIC_PROCESS) activity of each cell, which was visualized on the UMAP plots. MODULE_306.v2022.1.Hs.gmt and GOBP_LACTATE_METABOLIC_PROCESS.v2023.1.Hs.gmt were obtained from the Molecular Signatures Database. Subsequently, the AUC values were extracted, and the functional activity differences between NPC and OPC were compared using Wilcoxon test.

2.4. Differential expression and transcription factors

The FindMarkers function in Seurat (default parameters) was used to identify differentially expressed genes between NPC and OPC for each cell cluster. The differentially expressed genes were visualized using scRNAtoolVis (v0.0.5). Top3 highly expressed markers (adjusted $P < 0.05$ and logfc > 0.25) of each epithelial subgroup were identified using FindAllMarkers and tidyverse (v1.3.2), with Wilcoxon test as the statistical test. SCENIC (v1.3.1) was used to infer cell transcription factor activity based on the RcisTarget database. Heatmaps were generated to show the transcription factor activities of each cell cluster using pheatmap (v1.0.12).

2.5. Cell trajectory inference

Monocle (v2.26.0) was used to infer pseudotime trajectories of T cell subgroups to explore T cell differentiation trajectories in NPC and OPC. The counts matrix was extracted from the Seurat object and converted into a CellDataSet. Differentially expressed genes between cell clusters were identified using the differentialGeneTest function, with $q < 0.01$. Cells were ordered based on the differentially expressed genes, followed by trajectory reconstruction.

2.6. Chromosomal copy number variation and intercellular communication

To assess the malignancy of epithelial cells, we utilized the infercnv package (v1.14.2) to infer chromosomal copy number variations in epithelial cells. We extracted counts matrices and clustering information from the Seurat object, utilizing endothelial cells as reference for copy number variation inference, followed by denoising. For analyzing intercellular interactions, we employed CellPhoneDB software (v4.1.0). We focused on glycolysis-enhanced epithelial cells and lactate-metabolizing T cells, inferring intercellular communication networks based on their gene expression levels.

3. Results

3.1. Characterization of cellular heterogeneity and composition in NPC and OPC microenvironments

We obtained single-cell sequencing data for 10 cases of NPC and 10 cases of oropharyngeal squamous cell carcinoma (OPSCC) from the GEO database. The overall workflow of this study is depicted in Fig. 1A. After removing low-quality cells and potential doublets, a total of 122,891 cells were included in the subsequent analysis. Based on established markers from previous studies, we classified these 122,891 cells into seven distinct cell types, as depicted in the UMAP plot (Fig. 1B). These seven cell clusters comprise T/NK cells (marked by PTPRC, CD3D/E, CD4, CD8A, FCGR3A, NCAM1, and KLRF1), B cells (marked by CD19, CD79A, and MS4A1), myeloid cells (marked by CD68, LYZ, CD14, ITGAX, LAMP3, and CD163), mast cells (marked by TPSAB1), fibroblasts (marked by COL1A1, COL3A1, FGF7, and MME), epithelial cells (marked by EPCAM, KRT5, KRT18, and KRT19), and endothelial cells (marked by FLT1, VWF, and PECAM1).

Additionally, the UMAP plot (Fig. 1B) provides insight into the origin of these cells from specific patients and tumor types. The aggregation pattern of these cell types reveals inter-patient and intra-tumor heterogeneity, indicating varying compositions of the same tumor subtype among different patients. The expression distribution of marker genes

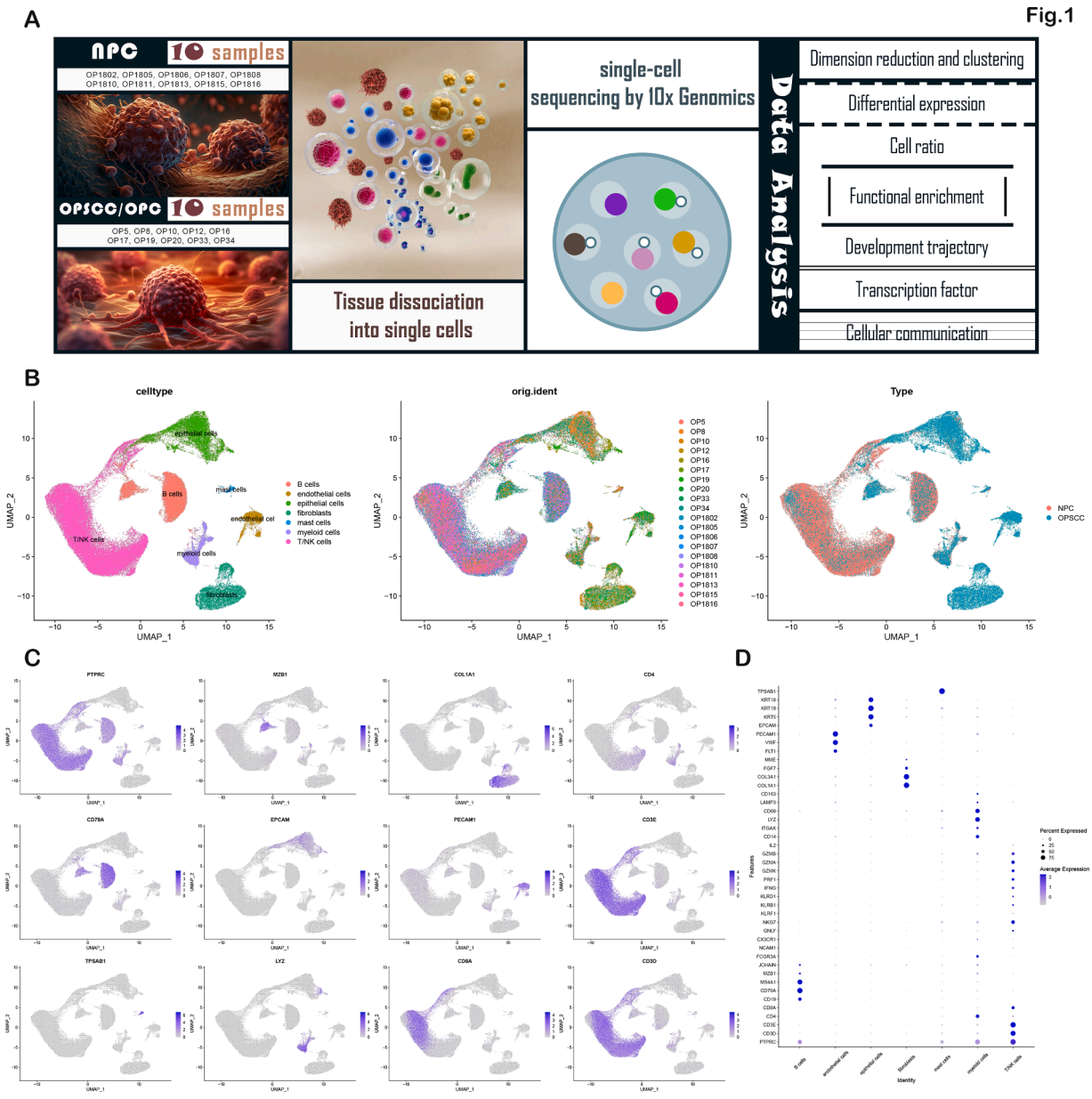

Fig. 1. Single-cell profiles of the NPC and OPC microenvironments. (A) Schematic representation of the research workflow. (B) UMAP plots depicting cell clusters (left), patients (center), and tumor types (right). Each dot represents a cell, and colors indicate different cell clusters (left), patients (center), and tumor types (right). (C) UMAP plots illustrating marker gene expression; color depth represents marker expression levels. (D) Marker expression of identified cell clusters; dot size indicates the percentage of cells highly expressing the marker, and color depth represents expression levels.

for these seven cell clusters is illustrated in Fig. 1C and D and Supplementary Fig. 1. Notably, substantial variations in the proportions of these seven cell clusters exist among individual patients, underscoring the presence of individual heterogeneity in both NPC and OPC and suggesting significant variability in the response to immune-targeted therapies among patients (Fig. 2A).

Distinct differences are observed in the cellular composition proportions between NPC and OPC. In NPC, T/NK cells and B cells are dominant, while in OPC, epithelial cells, endothelial cells, and fibroblasts predominate (Fig. 2B). Specifically, the proportion of T/NK cells ($P = 7.6e{-}05$) is higher in NPC compared to OPC. Conversely, the proportion of epithelial cells ($P = 4.3e{-}05$), myeloid cells ($P = 0.029$), fibroblasts ($P = 0.00017$), and endothelial cells ($P = 0.00016$) is higher in OPC compared to NPC (Fig. 2C).

3.2. Dynamic trajectory analysis of T cell development and transcription factors regulation in NPC and OPC microenvironments

Based on established markers from previous studies, we divided 65,253 T/NK cells into 19 clusters. One cluster labeled as 'unknown' was excluded as it potentially represented doublets (Fig. 3A and B). These 18 cell clusters encompass CD4_C1_ICOS/KLRB1, CD4_C2_CCR7, CD4_C3_KLRB1/CXCL13, Treg, CD8_C1_NKG7/HAVCR2, CD8_C2_NKG7/LAG3, CD8_C3_GZMK, CD8_C4_KLRD1, CD8_C5_NKG7/CD69, CD8_C6_GZMK/CD69, CD8_C7_GZMA/LAG3, CD8_C8_IL7R/NKG7, CD8_C9_STMN1/GZMB, CD8_C10_MKI67/GZMB, CD8_C11_GZMK/CXCL13, CD8_C12_TNFRSF9/TIGIT, NK, and CD4/CD8_DN.

These cell sources were visualized on a UMAP plot based on patient and tumor type (Fig. 3A). We then analyzed the expression profiles of specific CD4, CD8, and NK cell subgroups between NPC and OPC and identified five highly expressed and five low-expressed genes for each

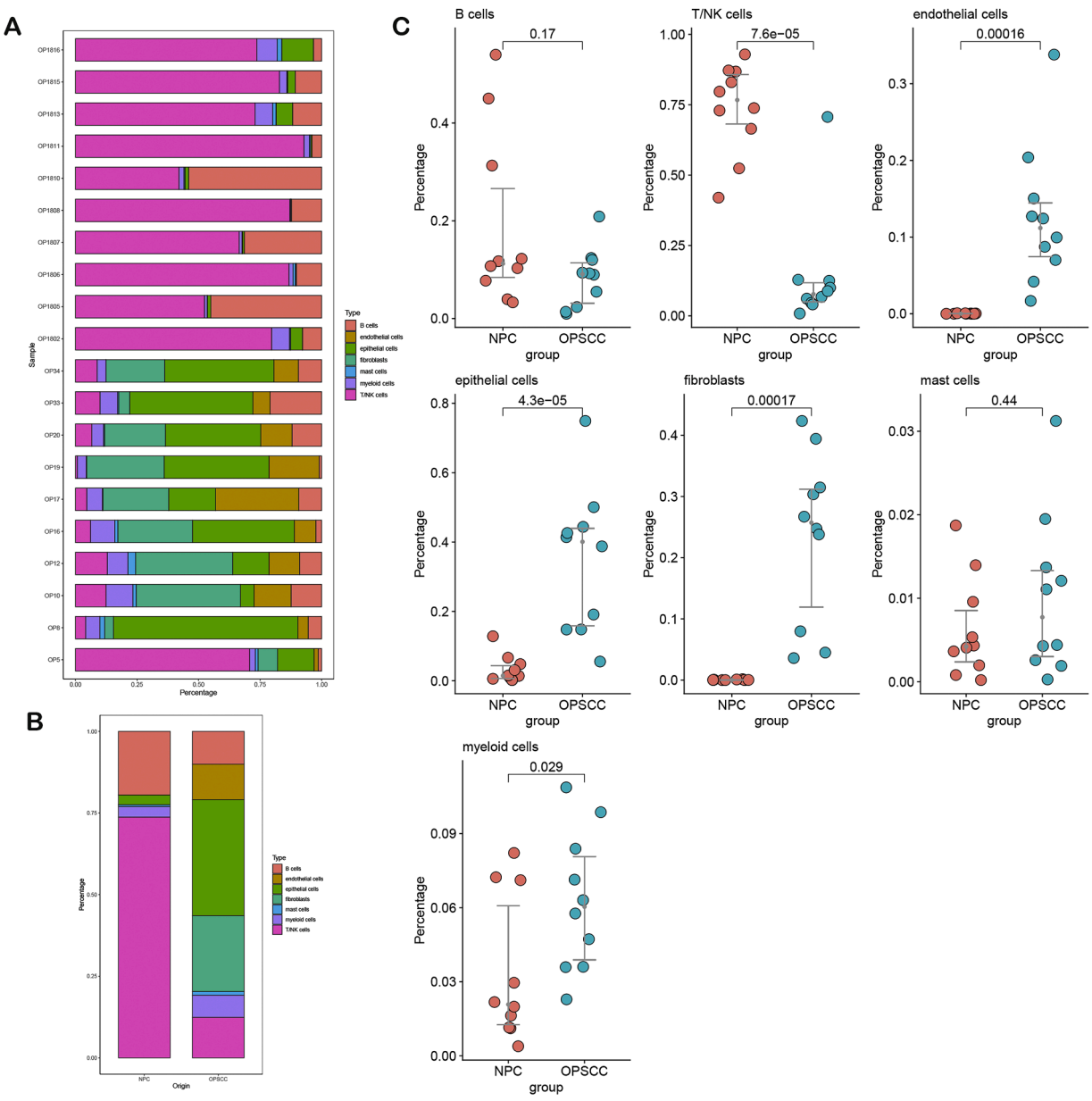

Fig. 2. Proportions of various cells in the NPC and OPC microenvironments. (A) Percentages of different cell types in each patient. (B) Cell composition percentages in NPC and OPC. (C) Proportional differences of cell clusters between NPC and OPC.

cell cluster in NPC compared to OPC (Fig. 3C). Subsequently, we conducted Gene Set Variation Analysis (GSVA), revealing that in OPC, these cells exhibit higher activity in the focal adhesion and metabolism of xenobiotics by cytochrome P450 pathways, while glycosylphosphatidylinositol GPI anchor biosynthesis, adipocytokine, and T cell receptor signaling pathways are more active in NPC. The aminoacyl TRNA biosynthesis pathway in the CD8_C12_TNFRSF9/TIGIT cell cluster remained active in both NPC and OPC (Fig. 3D).

We quantified the Cytotoxicity, Exhaustion, Naivety, and Proliferation scores for each cell using the AddModuleScore function. Notably, the CD8_C1_NKG7/HAVCR2, CD8_C2_NKG7/LAG3, and NK cell clusters showed higher cytotoxicity scores. CD8_C3_GZMK and CD8_C8_IL7R/NKG7 displayed higher cytotoxicity scores in NPC compared to OPC. In contrast, CD8_C1_NKG7/HAVCR2, CD8_C2_NKG7/LAG3, CD8_C4_KLRD1, CD8_C5_NKG7/CD69, and NK exhibited higher cytotoxicity scores in OPC than in NPC (Fig. 3E).

The CD8_C1_NKG7/HAVCR2 and CD8_C2_NKG7/LAG3 cell clusters exhibit higher exhaustion scores. CD8_C3_GZMK, CD8_C9_STMN1/GZMB, CD8_C10_MKI67/GZMB, and CD8_C12_TNFRSF9/TIGIT display higher exhaustion scores in NPC compared to OPC. In contrast, CD8_C2_NKG7/LAG3 and CD8_C4_KLRD1 exhibit higher exhaustion scores in OPC compared to NPC. The CD4_C2_CCR7 and CD8_C8_IL7R/NKG7 cell clusters show higher naïve scores. CD8_C9_STMN1/GZMB and CD8_C10_MKI67/GZMB cell clusters exhibit higher proliferation scores, with CD8_C9_STMN1/GZMB showing higher proliferation scores in OPC than in NPC, while CD8_C10_MKI67/GZMB exhibits higher proliferation scores in NPC than in OPC (Fig. S2A).

We conducted AUCell analysis using glycolysis and lactate-related genes. The CD8_C9_STMN1/GZMB and CD8_C10_MKI67/GZMB cell clusters actively participate in glycolysis and lactate metabolism processes. CD8_C9_STMN1/GZMB demonstrates lower activity in glycolysis ($P = 0.018$) and lactate metabolism ($P = 0.04766$) in NPC compared to OPC. CD8_C10_MKI67/GZMB exhibits higher activity in glycolysis ($P =$ 8.1e-12) and lactate metabolism ($P =$ 8.6e-08) in NPC compared to OPC (Fig. 4A). Distinct gene regulatory patterns exist among different cell clusters in different tumors, while similarities also emerge. In NPC, the

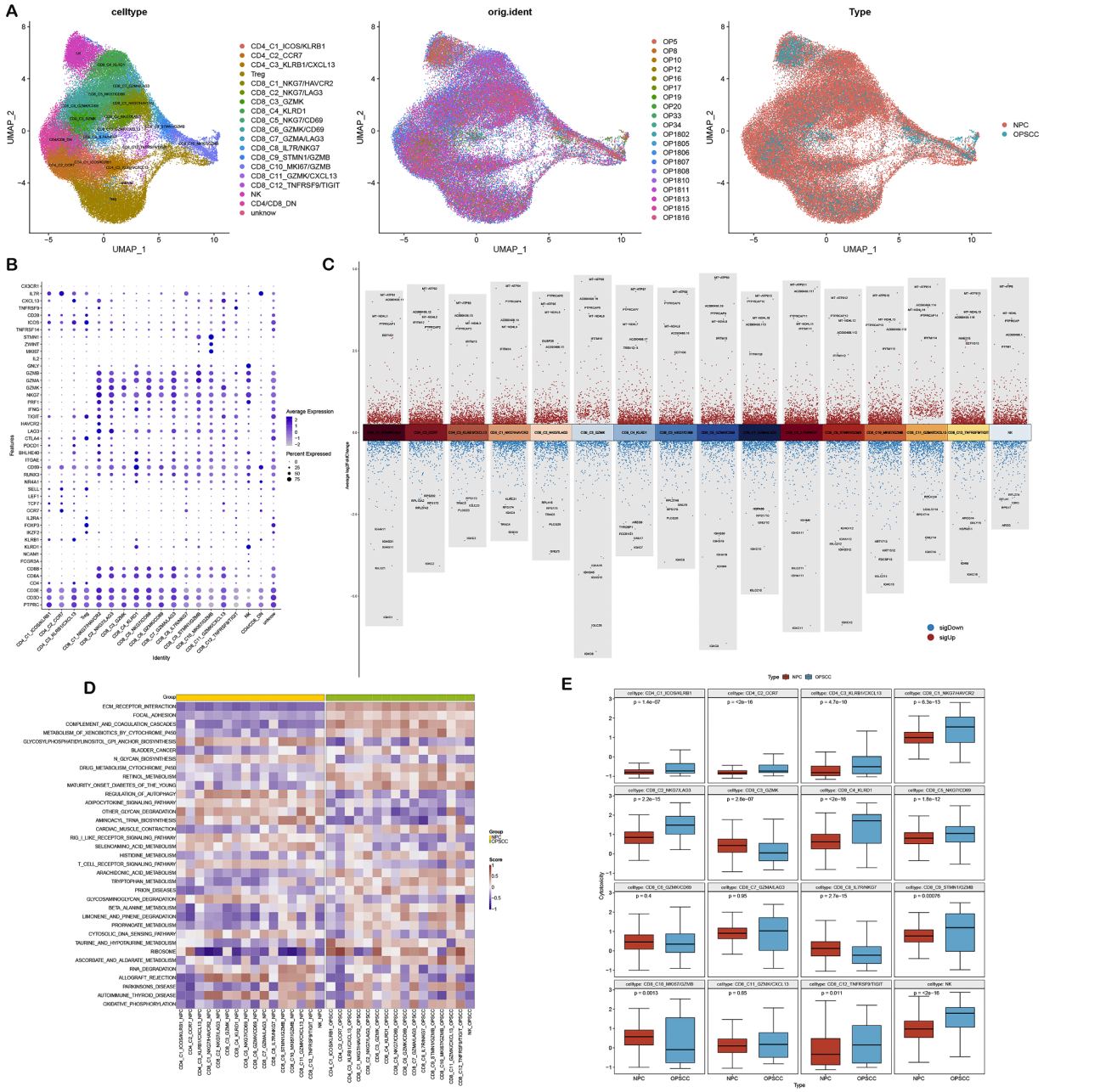

Fig. 3. Heterogeneity of T/NK cells in NPC and OPC. (A) UMAP plots illustrating T/NK cell clusters (left), patients (center), and tumor types (right). (B) Marker expression of identified T/NK cell clusters; dot size indicates the percentage of cells highly expressing the marker, and color depth represents expression levels. (C) Differential analysis (NPC vs OPC) of T/NK cells' gene expression. (D) Gene Set Variation Analysis (GSVA) depicting functional activity; yellow for NPC, green for OPC, dark blue to dark red for low to high functional activity. (E) Functional score comparison for cytotoxicity, with red indicating NPC and blue indicating OPC.

active transcription factors in CD8_C9_STMN1/GZMB are ENO1, whereas in CD8_C10_MKI67/GZMB, RAD21 and EZH2 are prominent. In OPC, active transcription factors in CD8_C9_STMN1/GZMB include YBX1, TFDP1, EZH2, BRCA1, and E2F1, while in CD8_C10_MKI67/GZMB, YBX1, CEBPD, RAD21, ID1, MAFB, NFIB, TFDP1, EZH2, BRCA1, E2F1, NFE2L2, and EGR1 are active (Fig. 4B). In NPC, STAT1 and IRF7 may exhibit co-expression, as might LEF1 and TCF7. In OPC, IRF7 and STAT1 may also demonstrate co-expression (Fig. 4C).

To elucidate the developmental trajectory of CD8 T cells within the NPC and OPC microenvironments, we selected CD8 T cell clusters with distinctive features and employed the monocle package for trajectory inference. Both in NPC and OPC, the CD8 T cell development begins with the double-negative T cell (CD4/CD8_DN) state, progressing to a terminal state with combined exhaustion and cytotoxicity (CD8_C1_NKG7/HAVCR2) and a cytotoxic proliferative state (CD8_C10_MKI67/GZMB). The trajectory analysis reveals a general progression of CD4/CD8_DN-immature T cells transitioning to cytotoxic (CD8_C8_IL7R/NKG7 or CD8_C3_GZMK) cells, followed by exhaustion (CD8_C4_KLRD1 or CD8_C5_NKG7/CD69 or CD8_C12_TNFRSF9/TIGIT), and subsequently, the abundant proliferation of cytotoxic T cells accompanied by exhaustion (CD8_C1_NKG7/HAVCR2 or CD8_C10_MKI67/GZMB) (Fig. 5A). We present heatmap depictions of the dynamic changes in the top 50 gene expression levels over time in NPC and OPC (Figs. 5B and S2C). Building upon our prior research indicating the impact of COPS5 expression on NPC patient prognosis[10,11], we investigated the temporal dynamics of the COPS gene family in both NPC and OPC. In NPC, the expression of COPS2, COPS5, and COPS6 initially increases and subsequently decreases over time, while COPS3 expression gradually

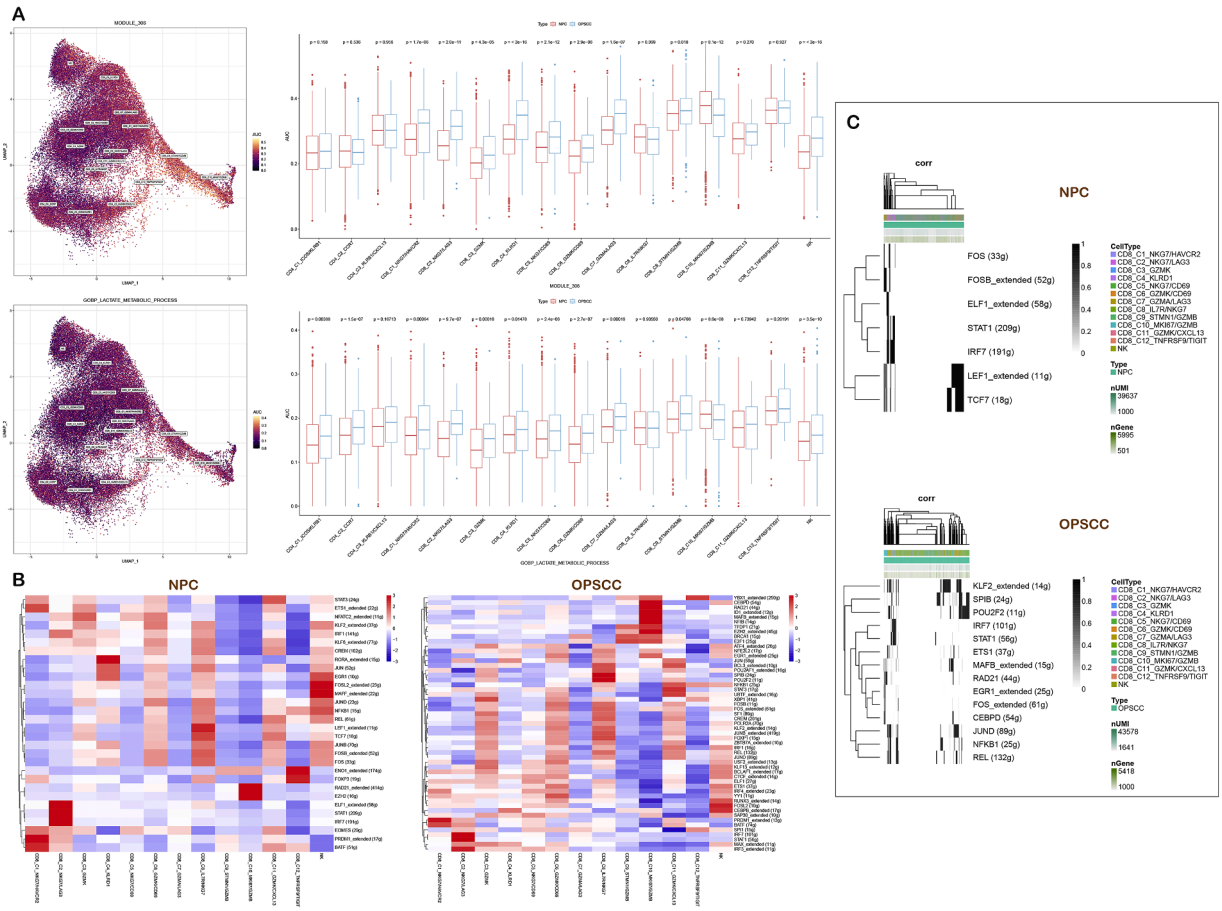

Fig. 4. Functional activity and transcription factors. (A) UMAP plots indicating glycolysis and lactate metabolic activity (left); differences in activity within each cell cluster (right). (B) Transcription factor activity in NPC and OPC. (C) Co-expression of transcription factors in NPC and OPC.

rises. In OPC, the expression of COPS3, COPS4, COPS5, COPS6, and COPS8 steadily increases over time (Figs. 5C and S2B).

3.3. *Diverse developmental trajectories and functional heterogeneity of treg cell subsets in NPC and OPC microenvironments*

We classified 11,728 Treg cells into five distinct clusters based on established markers from previous studies, including Treg_C1_DNAJB1, Treg_C2_ICOS, Treg_C3_SELL, Treg_C4_CD69, and Treg_C5_STMN1 (Fig. 6A). The origin of these cell clusters from specific patients and tumor types is depicted in Fig. 6A. The expression levels of marker genes in these cell clusters are illustrated in Fig. 6B. These Treg cell clusters exhibit heterogeneity among different patients, particularly evident in patient OP17 where Treg_C1_DNAJB1 and Treg_C5_STMN1 cell clusters predominate (Fig. S3A). In the context of NPC, the majority of Treg cells are classified as Treg_C2_ICOS, while in OPC, Treg_C1_DNAJB1 cells are more predominant (Fig. 6C). Specifically, the proportion of Treg_C1_DNAJB1 ($P = 0.00026$) is lower in NPC compared to OPC, whereas the proportion of Treg_C2_ICOS ($P = 0.00028$) is higher in NPC than in OPC (Fig. S3B).

Treg_C2_ICOS and Treg_C5_STMN1 cell clusters demonstrate strong glycolytic and lactate activity, with Treg_C2_ICOS exhibiting higher glycolysis ($P = 0.0068$) and lactate production ($P = 0.0218$) in OPC compared to NPC. Conversely, Treg_C5_STMN1 shows higher glycolysis activity ($P = 1.9e\text{-}05$) in NPC compared to OPC (Fig. 6D and E). Treg_C2_ICOS cell cluster exhibits elevated IL2R and exhaustion scores. In NPC, these five Treg cell clusters have higher IL2R and co-stimulation scores compared to OPC (Figs. 6F and S3C). The proliferative capacity of Treg_C5_STMN1 is higher, particularly in NPC ($P = 0.00026$). Treg_C3_SELL cell cluster shows higher naivety scores in NPC compared to OPC ($P = 0.0052$) (Fig. S3C). STAT1, IRF7, and REL are highly active in the Treg_C2_ICOS cell cluster, both in NPC and OPC microenvironments. Treg_C5_STMN1 cell cluster exhibits elevated activity of BRCA1 in both NPC and OPC (Fig. S3D). Co-regulation of IRF7 and STAT1 is suggested in both NPC and OPC Treg cell clusters. Additionally, in NPC, co-regulation of KLF2 and KLF3 is possible in Treg cell clusters (Fig. S3E).

The developmental trajectory of Treg cells in both NPC and OPC microenvironments initiates with Treg_C3_SELL, transitions through intermediate states represented by Treg_C1_DNAJB1, Treg_C2_ICOS, and Treg_C4_CD69, and culminates in the terminal state characterized by Treg_C5_STMN1 (Figs. 6G and S4A). The dynamic expression of the top 50 genes in Treg cells over time is displayed in Supplementary Fig. 4B for both NPC and OPC. In NPC, the expression of COPS3 increases over time, while the expression of COPS2, COPS5, COPS6, and COPS8 increases initially and then stabilizes. In contrast, in OPC, the expression of COPS3, COPS4, COPS6, and COPS8 increases over time, while COPS5 expression initially increases and then stabilizes (Fig. S4C).

3.4. *Delineating heterogeneity of malignant epithelial cells in NPC and OPC microenvironments*

We utilized endothelial cells as a reference to determine 17,103 malignant epithelial cells with chromosomal copy number variations in NPC and OPC. These cells were further categorized into 14 distinct clusters through unsupervised clustering (Fig. 7A and C). The origin of these cells from patients and tumors is illustrated in Fig. 7A. Considerable heterogeneity is observed in the composition and types of

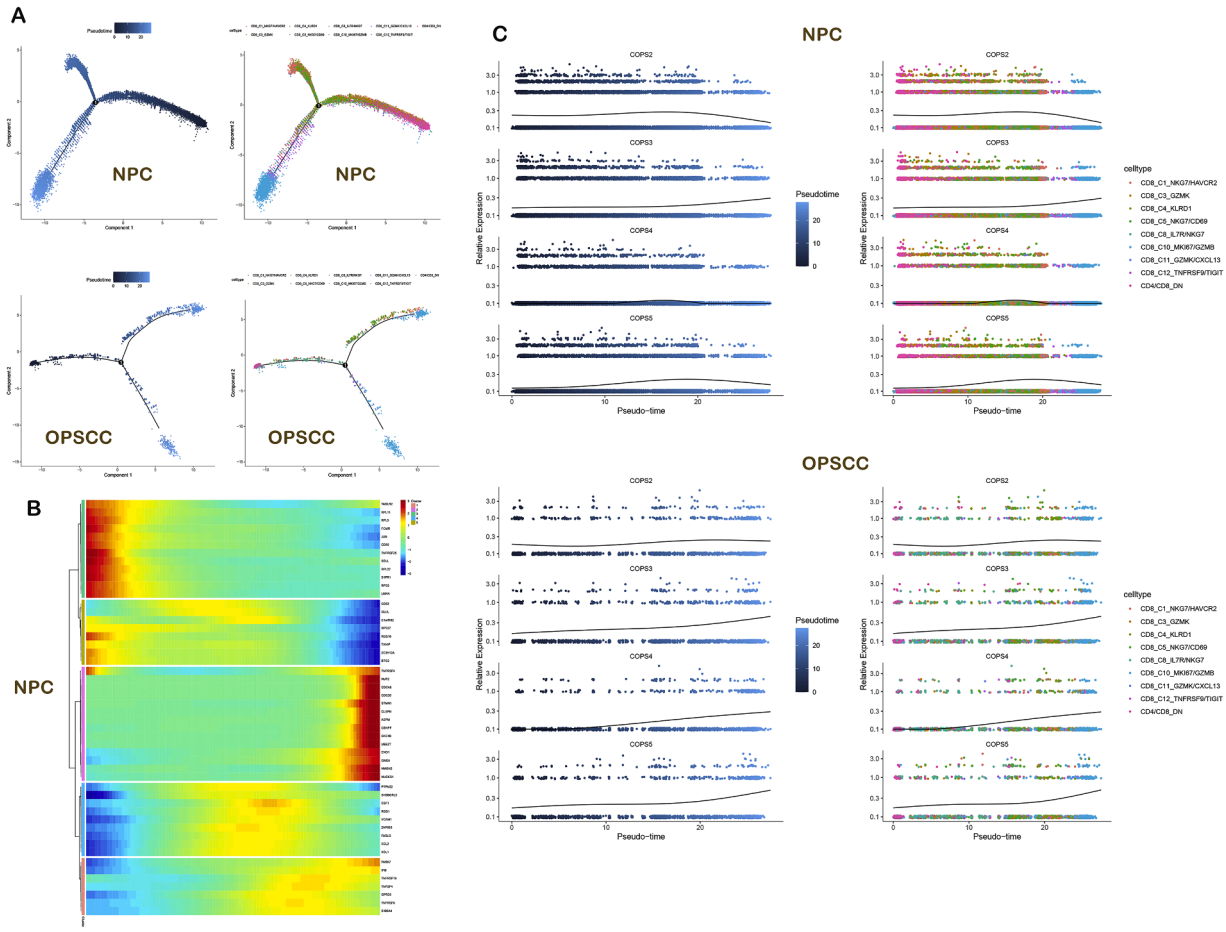

Fig. 5. Cell developmental trajectories inferred. (A) Developmental trajectory of representative CD8 T cell clusters. (B) Heatmap of dynamic expression of Top 50 genes over time in NPC. (C) Dynamic expression of COPS family genes over time in NPC and OPC.

malignant epithelial cells across individual patients, indicative of strong variability (Fig. S5A). Notably, in NPC, clusters 0 and 1 are dominant among malignant epithelial cells, whereas in OPC, a greater diversity of malignant epithelial cells is evident, with cluster 0 being more prominent (Fig. 7B). Top 3 highly expressed genes (Adjusted P-value < 0.05) were selected for each cluster of malignant epithelial cells based on avg_log2FC, as depicted in Fig. 7D. The differential gene expression profiles of these 14 clusters of malignant epithelial cells in NPC and OPC can be observed in Supplementary Fig. 5B."

Metabolic analysis reveals a general upregulation of glycolytic activity in all 14 clusters of malignant epithelial cells, with cluster 8 exhibiting particularly elevated glycolytic activity. Interestingly, cluster 8 in NPC demonstrates higher glycolytic activity than in OPC, although statistically insignificant (Fig. 7E and F). Pathway analysis indicates that unfolded protein response, mTORC1 signaling, MYC targets V2, and PI3K-AKT-mTOR signaling show increased activity in NPC compared to OPC. Cluster 12 of malignant epithelial cells exhibits robust activation of interferon gamma response and interferon alpha response, which is consistent in both NPC and OPC. Additionally, clusters 4, 7, and 9 show higher activity of interferon gamma response and interferon alpha response in NPC than in OPC (Fig. 8A).

3.5. Cell-cell interactions and metabolic signatures of malignant epithelial cells and immune cell subpopulations in NPC and OPC microenvironments

Enhanced glycolytic activity in cluster 8 malignant epithelial cells, while cluster CD8_C9_STMN1/GZMB and cluster CD8_C10_MKI67/GZMB exhibit elevated lactic acid metabolism. In both NPC and OPC, cluster 8 malignant epithelial cells engage in extensive interactions with CD8_C9_STMN1/GZMB and CD8_C10_MKI67/GZMB, as well as active interactions with Treg_C2_ICOS, Treg_C4_CD69, and Treg_C5_STMN1 (Fig. 8B). In both NPC and OPC, cluster 8 malignant epithelial cells interact with CD8_C9_STMN1/GZMB and CD8_C10_MKI67/GZMB through MIF-TNFRSF14. The interaction involves CD74 from CD8_C10_MKI67/GZMB and CD8_C9_STMN1/GZMB with MIF and APP from cluster 8 malignant epithelial cells in both NPC and OPC. In NPC, cluster 8 malignant epithelial cells interact with CD8_C9_STMN1/GZMB and CD8_C10_MKI67/GZMB via TNFSF15-TNFRSF25, which is absent in OPSCC. Additionally, in OPC, cluster 8 malignant epithelial cells interact with CD8_C9_STMN1/GZMB and CD8_C10_MKI67/GZMB via CXCL14-CXCR4, whereas this interaction is absent in NPC. CD8_C9_STMN1/GZMB in OPC engages with cluster 8 malignant epithelial cells through CD94:NKG2C-HLA-E and CD94:NKG2A-HLA-E interactions, which are not evident in NPC (Fig. 8C). In OPC, active interactions between cluster 8 malignant epithelial cells and Treg cell clusters are mediated by CD2-CD58, CD27-CD70, CD74-COPA, and CD74-MIF (Fig. S5C).

4. Discussion

Tumor heterogeneity is a critical factor contributing to the variability in therapeutic responses observed among different tumor patients[12]. Consequently, the significance of tumor microenvironments in diagnosis and treatment has garnered increasing attention, prompting the application of single-cell sequencing to unravel their intricate compositions. While preliminary studies have separately depicted cell atlases for NPC and OPC[13,14], a comprehensive exploration of the commonalities and heterogeneities between these anatomically

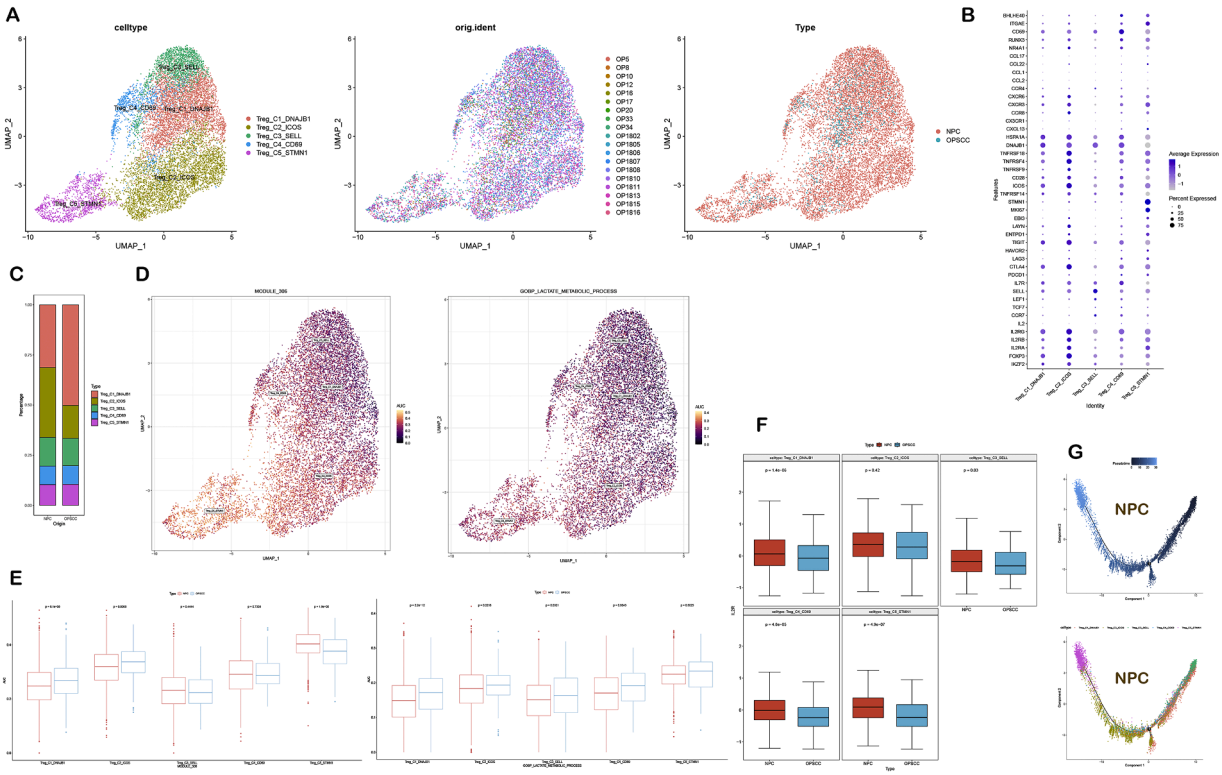

Fig. 6. Diversity of Treg cells in NPC and OPC. (A) UMAP plots depicting Treg cell clusters (left), patients (center), and tumor types (right). (B) Marker expression of identified Treg cell clusters; dot size indicates the percentage of cells highly expressing the marker, and color depth represents expression levels. (C) Proportional differences of Treg cell clusters between NPC and OPC. (D) UMAP plots indicating glycolysis and lactate metabolic activity. (E) Differences in glycolysis activity in each Treg cell cluster. (F) Functional score comparison for IL2R, with red indicating NPC and blue indicating OPC. (G) Developmental trajectory of Treg cell clusters in NPC.

adjacent tumors remains largely unaddressed. Our study sought to bridge this gap by elucidating the heterogeneity, metabolic signatures, and intercellular interactions that contribute to the distinct characteristics of these two types of head and neck cancers.

Our analysis revealed distinct cellular landscapes within the NPC and OPC microenvironments. Tumor microenvironment composition exhibited considerable variations, reflecting the inherent heterogeneity among individual patients. Notably, the dominance of T/NK and B cells in NPC, in contrast to the prevalence of epithelial cells, endothelial cells, and fibroblasts in OPC, underscores the intricate interplay between tumor origin and microenvironmental dynamics.

The observed transition of CD8 T cells from a naive state to cytotoxicity, accompanied by the gradual onset of exhaustion, holds pivotal implications. In both NPC and OPC, the coexistence of cytotoxic and exhausted CD8 T cell subsets signifies a dynamic process of immune response. This phenomenon, wherein activated T cells shift towards exhaustion without complete loss of function, aligns with prior reports in NPC [15]. Moreover, the heightened proliferative capacity of Tregs in the terminal states, accompanied by exhaustion, suggests their intricate role in shaping the microenvironment. In our investigation, we observed heightened proliferation of CD8 T and Treg cell clusters in both NPC and OPC, characterized by enhanced glycolysis and lactate metabolism activities. Tumor microenvironments often experience hypoxia, prompting tumor cells to engage in glycolysis for energy production and resulting in substantial lactate generation. This lactate, in turn, exerts regulatory effects on immune cell activity and functionality [16]. Despite the initial presence of ample oxygen during early tumor formation, tumor cells, including rapidly proliferating cells like effector T cells, can also undergo aerobic glycolysis [17]. Prior research has indicated that activated T cells can fulfill their nutritional demands by converting glucose to lactate through glycolysis or aerobic glycolysis [18]. Notably, extracellular lactate levels closely correlate with T cell proliferation [19]. Tregs utilize lactate for proliferation to sustain their immunosuppressive functions, induce PD-1 expression, and potentially inhibit the cytotoxicity of effector T cells[20,21].

A fascinating hypothesis emerges from our findings, suggesting that malignant epithelial cells and T cells may resort to glycolysis or aerobic glycolysis to meet their energy requirements and generate substantial lactate. Over time, glucose depletion due to extensive consumption by these cells may lead to low glucose concentrations in the microenvironment, consequently resulting in substantial lactate accumulation. Furthermore, as both malignant epithelial cells and T cells necessitate energy for their metabolic processes, they might rely on the accumulated lactate within the microenvironment. Within the context of our study, we have unveiled that highly glycolytic malignant epithelial cells interact with lactate-producing and glycolysis-enriched proliferative effector T cells through MIF-TNFRSF14, MIF-CD74, and APP-CD74 interactions in both NPC and OPC. Interestingly, these proliferative effector T cells are concurrently marked by exhaustion.

Previous studies have indicated that the MIF/CD74 axis in murine hepatocellular carcinoma promotes tumor proliferation while exerting anti-apoptotic effects[22]. Activation of the MIF-CD74 axis induces highly proliferative, low-differentiated, and low-activity memory B cells in hepatocellular carcinoma [23]. In the microenvironment of Cutaneous T cell lymphoma, interactions between CCL13+ monocyte-derived macrophages and LAMP3+cDC cells through MIF-CD74 contribute to immune suppression by engaging malignant T cells [24]. Moreover, interactions involving APP-CD74 have been documented between malignant epithelial cells and T cells in adenoid cystic carcinoma [25]. In the context of NPC and OPC, strongly glycolytic malignant epithelial cells interact with lactate-producing and glycolysis-enriched proliferative T cells through MIF-TNFRSF14,

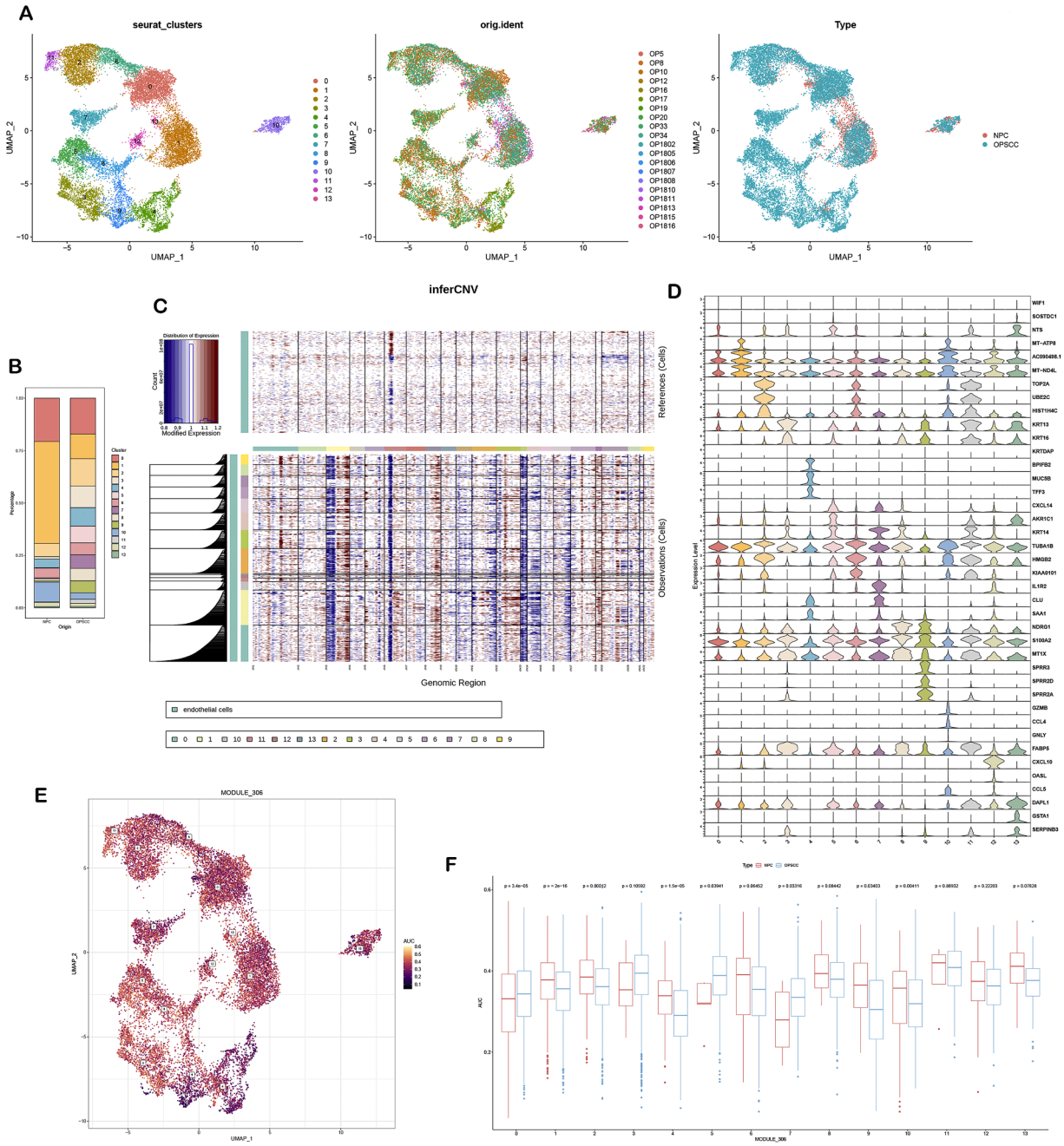

Fig. 7. Heterogeneity of malignant epithelial cells in NPC and OPC. (A) UMAP plots depicting malignant cell clusters (left), patients (center), and tumor types (right). (B) Proportional differences of malignant epithelial cell clusters between NPC and OPC. (C) Copy number variation inferred with reference to endothelial cells. (D) Top3 gene expression of each malignant cell cluster. (E) Glycolysis activity in each malignant cell cluster.

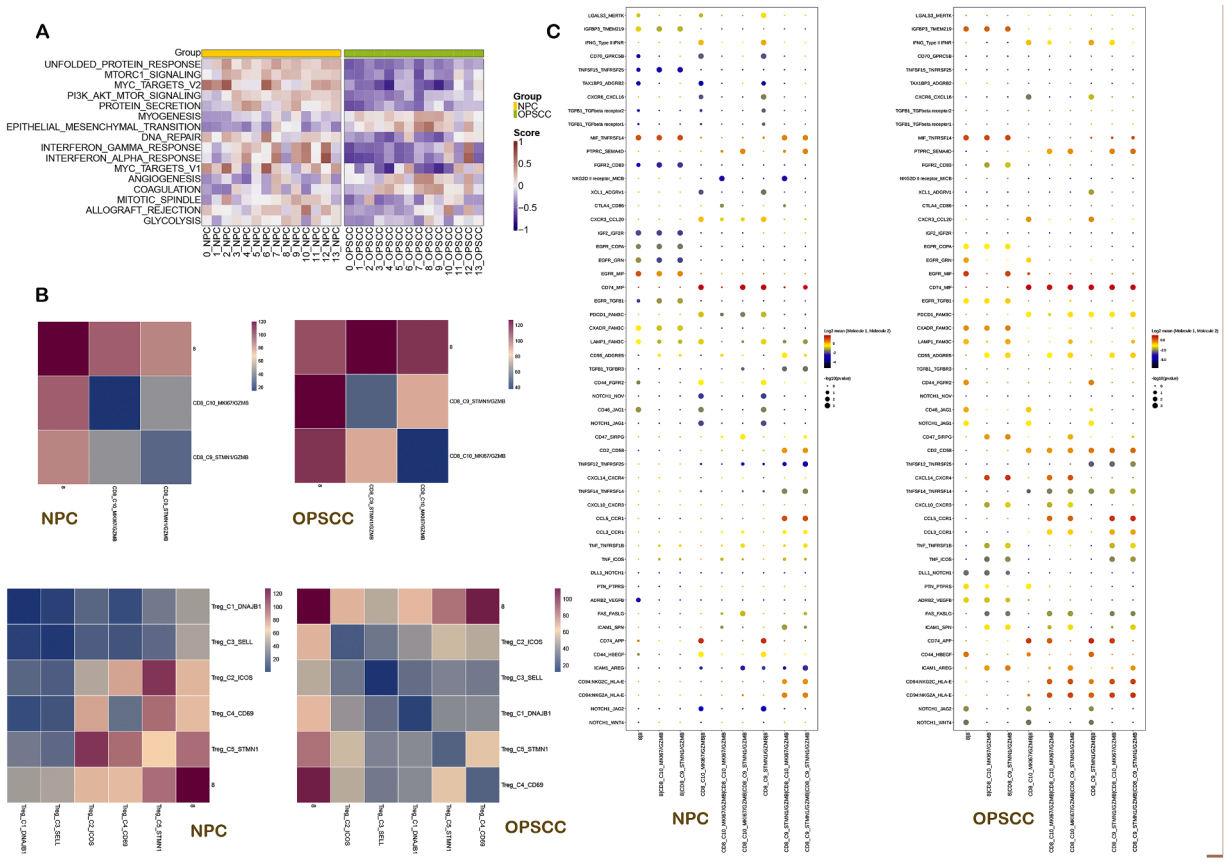

Fig. 8. Intercellular communication. (A) GSVA depicting functional activity. (B) Heat map indicating the number of intercellular interactions in NPC and OPC. (C) Interactions between two cell clusters through ligand-receptors in NPC and OPC, with color representing average expression and circle size representing P-value significance.

MIF-CD74, and APP-CD74 interactions. The exploration of the relationships between these metabolites and their respective ligands warrants further investigation. Furthermore, the potential co-expression of IRF7 and STAT1 in CD8 T cells, NK cells, and Tregs within NPC and OPC microenvironments necessitates deeper molecular investigations.

In conclusion, our single-cell sequencing analysis offers a comprehensive exploration of the cellular heterogeneity, metabolic signatures, and intercellular communication networks within the tumor microenvironments of NPC and OPC. The distinct characteristics observed in these two types of head and neck cancers provide valuable insights into their underlying biology and potential therapeutic avenues.

Ethic statement

Approval of the research protocol: N/A.
Informed Consent: N/A.
Registry and the Registration: N/A.
Animal Studies: N/A.

CRediT authorship contribution statement

Liping Wang: Methodology, Data curation, Writing – original draft. **Shuang Li:** Validation, Data curation. **Xinran Li:** Validation, Data curation. **Guangzheng Zhuo:** Validation, Data curation. **Qian Zhang:** Data curation. **Guohong Liu:** Validation, Data curation, Funding acquisition. **Yunbao Pan:** Conceptualization, Supervision, Writing – review & editing, Funding acquisition.

Declaration of competing interest

The authors declare that they have no known competing financial interests or personal relationships that could have appeared to influence the work reported in this paper.

Data availability

The original contributions presented in the study are included in the article. Further inquiries can be directed to the corresponding authors.

Funding

This work was supported by the National Natural Science Foundation of China (81872200, 31900558), the Hubei Provincial Youth Talents Program for Public Health (WSJKRC2022013), Wuhan Young and middle-aged medical backbone talents Training Project (WHQG201904), the Yellow Crane Talent Program of Wuhan City (HHYC2019002), the Natural Science Foundation of Hubei Province (2020CFB298), the Zhongnan Hospital of Wuhan University Science, Technology and Innovation Seed Fund (ZNPY2018090, ZNPY2019002).

Supplementary materials

Supplementary material associated with this article can be found, in the online version, at doi:10.1016/j.neo.2024.100980.

References

[1] V. Van den Bossche, H. Zaryouh, M. Vara-Messler, J. Vignau, J.P. Machiels, A. Wouters, S. Schmitz, C. Corbet, Microenvironment-driven intratumoral heterogeneity in head and neck cancers: clinical challenges and opportunities for precision medicine, Drug Resist. Updat. 60 (2022) 100806.

[2] J.M. Argiles, F.J. Lopez-Soriano, B. Stemmler, S. Busquets, Cancer-associated cachexia - understanding the tumour macroenvironment and microenvironment to improve management, Nat. Rev. Clin. Oncol. 20 (2023) 250–264.

[3] K.C.W. Wong, E.P. Hui, K.W. Lo, W.K.J. Lam, D. Johnson, L. Li, Q. Tao, K.C. A. Chan, K.F. To, A.D. King, B.B.Y. Ma, A.T.C. Chan, Nasopharyngeal carcinoma: an evolving paradigm, Nat. Rev. Clin. Oncol. 18 (2021) 679–695.

[4] J.J. Kang, Y. Yu, L. Chen, K. Zakeri, D.Y. Gelblum, S.M. McBride, N. Riaz, C.J. Tsai, A. Kriplani, T.K.W. Hung, J.V. Fetten, L.A. Dunn, A.L. Ho, J.O. Boyle, I.S. Ganly, B. Singh, E.J. Sherman, D.G. Pfister, R.J. Wong, N.Y. Lee, Consensuses, controversies, and future directions in treatment deintensification for human papillomavirus-associated oropharyngeal cancer, CA Cancer J. Clin. 73 (2023) 164–197.

[5] M. Lechner, J. Liu, L. Masterson, T.R. Fenton, HPV-associated oropharyngeal cancer: epidemiology, molecular biology and clinical management, Nat. Rev. Clin. Oncol. 19 (2022) 306–327.

[6] W. Li, X. Duan, X. Chen, M. Zhan, H. Peng, Y. Meng, X. Li, X.Y. Li, G. Pang, X. Dou, Immunotherapeutic approaches in EBV-associated nasopharyngeal carcinoma, Front. Immunol. 13 (2022) 1079515.

[7] Y. Huang, Y. Lan, Z. Zhang, X. Xiao, T. Huang, An update on the immunotherapy for oropharyngeal squamous cell carcinoma, Front. Oncol. 12 (2022) 800315.

[8] K.C.W. Wong, D. Johnson, E.P. Hui, R.C.T. Lam, B.B.Y. Ma, A.T.C. Chan, Opportunities and challenges in combining immunotherapy and radiotherapy in head and neck cancers, Cancer Treat. Rev. 105 (2022) 102361.

[9] P. Goon, M. Schurmann, F. Oppel, S. Shao, S. Schleyer, C.J. Pfeiffer, I. Todt, F. Brasch, L.U. Scholtz, M. Goerner, H. Sudhoff, Viral and clinical oncology of head and neck cancers, Curr. Oncol. Rep. 24 (2022) 929–942.

[10] L. Wang, D. Wang, L. Yang, X. Zeng, Q. Zhang, G. Liu, Y. Pan, Cuproptosis related genes associated with Jab1 shapes tumor microenvironment and pharmacological profile in nasopharyngeal carcinoma, Front. Immunol. 13 (2022) 989286.

[11] L. Wang, X. Zeng, G. Yang, G. Liu, Y. Pan, Pan-cancer analyses of Jab1/COPS5 reveal oncogenic role and clinical outcome in human cancer, Heliyon. 8 (2022) e12553.

[12] M.R. Junttila, F.J. de Sauvage, Influence of tumour micro-environment heterogeneity on therapeutic response, Nature 501 (2013) 346–354.

[13] L. Wang, D. Wang, X. Zeng, Q. Zhang, H. Wu, J. Liu, Y. Wang, G. Liu, Y. Pan, Exploration of spatial heterogeneity of tumor microenvironment in nasopharyngeal carcinoma via transcriptional digital spatial profiling, Int. J. Biol. Sci. 19 (2023) 2256–2269.

[14] S.V. Puram, M. Mints, A. Pal, Z. Qi, A. Reeb, K. Gelev, T.F. Barrett, S. Gerndt, P. Liu, A.S. Parikh, S. Ramadan, T. Law, E.A. Mroz, J.W. Rocco, D. Adkins, W.L. Thorstad, H.A. Gay, L. Ding, R.C. Paniello, P. Pipkorn, R.S. Jackson, X. Wang, A. Mazul, R. Chernock, J.P. Zevallos, J. Silva-Fisher, I. Tirosh, Cellular states are coupled to genomic and viral heterogeneity in HPV-related oropharyngeal carcinoma, Nat. Genet. 55 (2023) 640–650.

[15] L. Gong, D.L. Kwong, W. Dai, P. Wu, S. Li, Q. Yan, Y. Zhang, B. Zhang, X. Fang, L. Liu, M. Luo, B. Liu, L.K. Chow, Q. Chen, J. Huang, V.H. Lee, K.O. Lam, A.W. Lo, Z. Chen, Y. Wang, A.W. Lee, X.Y. Guan, Comprehensive single-cell sequencing reveals the stromal dynamics and tumor-specific characteristics in the microenvironment of nasopharyngeal carcinoma, Nat. Commun. 12 (2021) 1540.

[16] Y. Gao, H. Zhou, G. Liu, J. Wu, Y. Yuan, A. Shang, Tumor microenvironment: lactic acid promotes tumor development, J. Immunol. Res. 2022 (2022) 3119375.

[17] L. Ye, Y. Jiang, M. Zhang, Crosstalk between glucose metabolism, lactate production and immune response modulation, Cytok. Grow. Fact. Rev. 68 (2022) 81–92.

[18] H. Chen, T. Yang, L. Zhu, Y. Zhao, Cellular metabolism on T-cell development and function, Int. Rev. Immunol. 34 (2015) 19–33.

[19] J.T. Grist, L.B. Jarvis, Z. Georgieva, S. Thompson, H. Kaur Sandhu, K. Burling, A. Clarke, S. Jackson, M. Wills, F.A. Gallagher, J.L. Jones, Extracellular lactate: a novel measure of T cell proliferation, J. Immunol. 200 (2018) 1220–1226.

[20] M.J. Watson, P.D.A. Vignali, S.J. Mullett, A.E. Overacre-Delgoffe, R.M. Peralta, S. Grebinoski, A.V. Menk, N.L. Rittenhouse, K. DePeaux, R.D. Whetstone, D.A. A. Vignali, T.W. Hand, A.C. Poholek, B.M. Morrison, J.D. Rothstein, S.G. Wendell, G.M. Delgoffe, Metabolic support of tumour-infiltrating regulatory T cells by lactic acid, Nature 591 (2021) 645–651.

[21] S. Kumagai, S. Koyama, K. Itahashi, T. Tanegashima, Y.T. Lin, Y. Togashi, T. Kamada, T. Irie, G. Okumura, H. Kono, D. Ito, R. Fujii, S. Watanabe, A. Sai, S. Fukuoka, E. Sugiyama, G. Watanabe, T. Owari, H. Nishinakamura, D. Sugiyama, Y. Maeda, A. Kawazoe, H. Yukami, K. Chida, Y. Ohara, T. Yoshida, Y. Shinno, Y. Takeyasu, M. Shirasawa, K. Nakama, K. Aokage, J. Suzuki, G. Ishii, T. Kuwata, N. Sakamoto, M. Kawazu, T. Ueno, T. Mori, N. Yamazaki, M. Tsuboi, Y. Yatabe, T. Kinoshita, T. Doi, K. Shitara, H. Mano, H. Nishikawa, Lactic acid promotes PD-1 expression in regulatory T cells in highly glycolytic tumor microenvironments, Cancer Cell 40 (2022) 201–218, e209.

[22] T.H. Wirtz, A. Saal, I. Bergmann, P. Fischer, D. Heinrichs, E.F. Brandt, M.T. Koenen, S. Djudjaj, K.M. Schneider, P. Boor, R. Bucala, R. Weiskirchen, J. Bernhagen, C. Trautwein, M.L. Berres, Macrophage migration inhibitory factor exerts pro-proliferative and anti-apoptotic effects via CD74 in murine hepatocellular carcinoma, Br. J. Pharmacol. 178 (2021) 4452–4467.

[23] Y. Bai, D. Chen, C. Cheng, Z. Li, H. Chi, Y. Zhang, X. Zhang, S. Tang, Q. Zhao, B. Ang, Y. Zhang, Immunosuppressive landscape in hepatocellular carcinoma revealed by single-cell sequencing, Front. Immunol. 13 (2022) 950536.

[24] Y. Du, Y. Cai, Y. Lv, L. Zhang, H. Yang, Q. Liu, M. Hong, Y. Teng, W. Tang, R. Ma, J. Wu, J. Wu, Q. Wang, H. Chen, K. Li, J. Feng, Single-cell RNA sequencing unveils the communications between malignant T and myeloid cells contributing to tumor growth and immunosuppression in cutaneous T-cell lymphoma, Cancer Lett. 551 (2022) 215972.

[25] P.G. An, W.J. Wu, Y.F. Tang, J. Zhang, Single-cell RNA sequencing reveals the heterogeneity and microenvironment in one adenoid cystic carcinoma sample, Funct. Integr. Genom. 23 (2023) 155.